analytical chemistry

pubs.acs.org/ac Article

Skipping the Boundary Layer: High-Speed Droplet-Based Immunoassay Using Rayleigh Acoustic Streaming

Qi Wang, Zhe Ding, Gary Wong,* Jia Zhou,* and Antoine Riaud*

Cite This: *Anal. Chem.* 2023, 95, 6253−6260 Read Online

ACCESS | Metrics & More | Article Recommendations | Supporting Information

ABSTRACT: Acoustic mixing of droplets is a promising way to implement biosensors that combine high speed and minimal reagent consumption. To date, this type of droplet mixing is driven by a volume force resulting from the absorption of high-frequency acoustic waves in the bulk of the fluid. Here, we show that the speed of these sensors is limited by the slow advection of analyte to the sensor surface due to the formation of a hydrodynamic boundary layer. We eliminate this hydrodynamic boundary layer by using much lower ultrasonic frequencies to excite the droplet, which drives a Rayleigh streaming that behaves essentially like a slip velocity. At equal average flow velocity in the droplet, both experiment and three-dimensional simulations show that this provides a three-fold speedup compared to Eckart streaming. Experimentally, we further shorten a SARS-CoV-2 antibody immunoassay from 20 min to 40 s taking advantage of Rayleigh acoustic streaming.

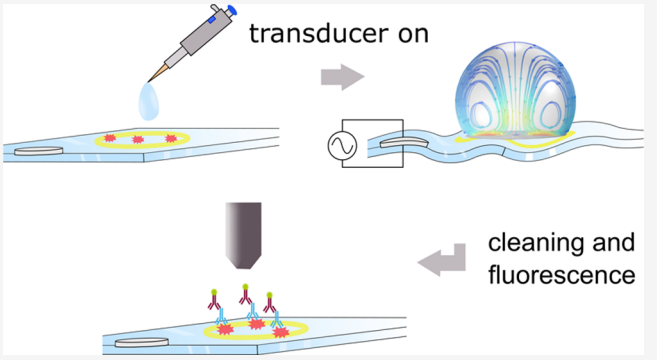

Downloaded via FUDAN UNIV on November 7, 2023 at 07:09:13 (UTC).
See https://pubs.acs.org/sharingguidelines for options on how to legitimately share published articles.

INTRODUCTION

Surface biosensors integrated in microfluidic devices enable the fast detection of molecules in small liquid samples. However, they face a trade-off between detection speed and sample waste. Indeed, the detection of dilute molecules by surface biosensors proceeds in three steps: the mass transfer of analyte from the bulk of the sample to the sensor surface, the adsorption of the analyte on the sensor surface (which can be made specific using antibody, DNA hybridization, or molecular imprints) and the detection of the adsorbed analyte (by fluorescence, surface plasmon resonance (SPR), field-effect transistor, and so on). Most often, mass transfer is the slowest step of all, and therefore determines the detection speed of the sensor.[1−3] This slow mass-transfer is mainly due to the formation of a concentration boundary layer that prevents the analytes from the bulk to reach the sensor. The thickness of this boundary layer can be decreased by introducing convection (mixing). However, for the simplest devices such as a biosensor embedded in a microchannel, increasing the flow rate also increases the waste of analyte[1] and the resulting shear may also damage the sensor.[3]

The mixing of sessile droplets (Figure 1) is a promising strategy to address this trade-off between detection speed and waste. On the one hand, convection ensures a negligible boundary layer thickness (fast mass transfer) and on the other hand, the batch-mode mixing ensures recycling of the outgoing fluid. Such droplets can be mixed using electrowetting actuation,[4] thermo-electric convection,[5] Marangoni effect,[6] or acoustic streaming (AS),[7] with the latter featuring high flow

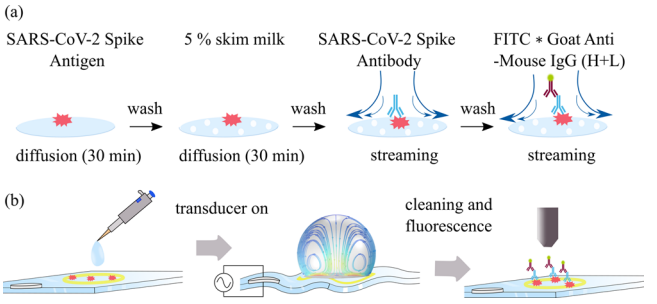

Figure 1. Accelerated SARS-CoV-2 antibody detection immunoassay. (a) Main steps of the immunoassay: spike proteins of the virus are deposited on a treated glass substrate, then skim milk is added to prevent nonspecfic adsorption. The analyte (primary antibody) can bind to the antigen is remains on the surface despite washing. Finally, the analyte is detected by a secondary fluorescent antibody. During the latest two stages, the mass transfer of antibodies to the sensor surface can be accelerated by mixing the liquid. (b) Method for the ultrasonic mixing: a droplet is deposited on the biosensor. When the transducer is turned on, the ultrasonic agitation of the glass is transmitted to the liquid, which triggers a steady Rayleigh acoustic streaming. After experiment, the glass slide is washed and the substrate fluorescence is measured by microscopy.

Received: September 4, 2022
Accepted: March 13, 2023
Published: April 5, 2023

© 2023 American Chemical Society

https://doi.org/10.1021/acs.analchem.2c03877
Anal. Chem. 2023, 95, 6253−6260

speed, the ability to mix pinned droplets (which is not possible for electrowetting), excellent biocompatibility and insensitivity to fluid composition and viscosity. Acoustic streaming has been observed in blood,[8] plasma,[8] serum,[9,10] saliva,[10] and urine.[11]

Acoustic streaming results from the transfer of pseudomomentum from an acoustic wave to the fluid, which can happen through two mechanisms:[12,13] due to the viscous attenuation of the wave in the bulk (Eckart streaming[14]) and due to the ultrasonic shear near the droplet boundaries (Rayleigh streaming).[15−17] Eckart streaming is easily generated using high-frequency surface acoustic waves (SAW) ultrasonic transducers (interdigitated transducers) and behaves like a volume force that can mix droplets[18] and, therefore, accelerate surface bioassays such as DNA hybridization assays,[7] immunoassays,[19] and SPR detection.[20] However, while Eckart streaming can reduce the thickness of the concentration boundary layer by stirring the droplet, the no-slip boundary condition at the solid−liquid interface creates a slow-moving hydrodynamic boundary layer near the sensor surface. As a result, the mixing improvement is limited by the slow convection near the solid wall.[21,22]

Unlike Eckart streaming, Rayleigh streaming behaves like a slip velocity that reaches an asymptotic value within a few micrometers from the surface,[15−17] as shown in Figure 2 (a).

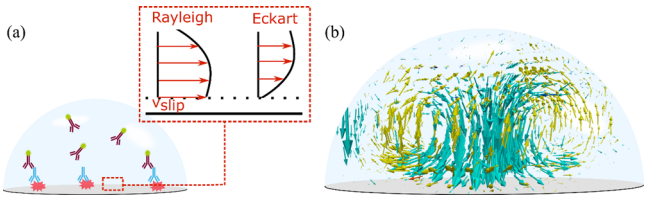

Figure 2. Acoustic streaming velocity fields. (a) Main difference between Eckart and Rayleigh streaming. Rayleigh streaming velocity is nonzero even within a few micrometers from the biosensor surface, whereas Eckart streaming features a hydrodynamic boundary layer due to the no-slip boundary condition on the sensor surface. (b) Experimental Rayleigh acoustic streaming field. To facilitate visualization, yellow and green arrows represent upward and downward velocities, respectively.

In this regard, it obliterates the hydrodynamic boundary layer near the sensor, and therefore ensures a faster detection at equal average flow velocity in the droplet. In most studies, Rayleigh streaming is created by oscillating sharp edges[23−25] or microbubbles,[26−28] and therefore the slip boundary condition is limited to the surface of the edges and bubbles. Instead, when considering surface biosensing applications, the slip velocity should occur on the sensor itself to maximize the detection speed. Accelerated detection of antibodies in both serum and saliva has been reported with Rayleigh streaming.[10] Although this type of full-device Rayleigh streaming has been achieved in microfluidic channels with hard-boundaries,[29] we are not aware of studies where it would have been applied to droplets in order to accelerate surface biosensing.

In this paper, we develop a microfluidic chip to expedite surface bioassays by mixing droplets without contact. Unlike previous studies based on Eckart streaming, using Rayleigh streaming eliminates the hydrodynamic boundary layer at the bottom of the droplet and accelerates analyte mass transfer to the sensor, which shortens the detection time compared to Eckart streaming with the same average flow velocity in the droplet. We first use finite element simulation to show that mass transfer with Rayleigh streaming is faster than with Eckart streaming at equal flow velocity in the droplet, and then verify this enhancement in experiments. Finally we use this Rayleigh streaming to shorten immunoassays from 20 min to just 40 s.

METHODS

Our experiment (Figure 1(a)) aims to detect the presence of SARS-CoV-2 antibodies (thereafter referred as the analyte). The biosensor is first coated with SARS-CoV-2 spike proteins (the antigen). The analyte then binds with the recombinant spike protein from SARS-CoV-2, and is subsequently detected with a secondary antibody (FITC * Goat anti-mouse IgG). The mass transfer of species to the surface can be accelerated by mixing the droplet with Rayleigh acoustic streaming (Figure 1(b)). A piezoelectric disc excited by an alternating voltage transmits its vibration to the droplet by the mean of a glass slide. Nonlinear interactions between the fluid and the solid then result in a steady flow in the droplet: the Rayleigh acoustic streaming. Eventually, the droplet is rinsed and the adsorbed species are observed by fluorescence microscopy.

Materials and Chemicals. Fluorescence microparticles were purchased from Huge Biotechnology (China), 2019-nCoV (SARS-CoV-2) Spike (S) Protein (His-Avi) was purchased from Yazyme Biomedical Technology Co. (CG202−01; China), SARS-CoV-2 (2019-nCoV) Spike Neutralizing Antibody was purchased from Sino Biological (40591-MM43; China), FITC * Goat Anti-Mouse IgG(H+L) was provided by Beyotime Biotechnology (A0568; China), 3-APTES toluene solution was provided by Aladdin Bio-Chem Technology (A107147; China), and toluene and methanol were provided by Sinopharm (10022818 and 10014108, respectively; China). All chemicals and reagents were used as received without further purification. The piezoelectric disc (1 MHz resonance frequency, 20 mm diameter) was purchased from Shanghai Daobo Electric Co., Ltd and the glass substrate was purchased from Foshan Yuanjingmei Glass Co., Ltd. The $LiNbO_3$ wafer was purchased from RDMICRO (China).

Surface Chemistry. Most experiments use glass slides and the remaining are performed on SiO_2-coated lithium niobate. Except for structure properties (which were not tested), the SiO_2 coating is chemically similar to glass. For convenience, both substrates (glass and SiO_2 coating) will be referred to as glass in the remaining of the surface chemistry section. The glass slides are first functionalized with 3-aminopropyl triethoxysilane (3-APTES) to enable the binding of proteins. The functionalized substrate is then used either to measure the mass transfer of fluorescent antibodies (FITC * Goat Anti-Mouse lgG (H+L)) or to perform an immunoassay.

Preparation of APTES-Functionalized Glass Slides. A clean glass surface is first activated (hydroxilated) by treating it for 3 min with an air plasma. The activated surface is then silanized by immersion in a 20 mM 3-APTES toluene solution overnight. Finally, the substrate is rinsed with toluene and methanol to remove the unbounded 3-APTES.

Mass Transfer Assay. A 0.2 mg/mL FITC * Goat Anti-Mouse lgG (H+L)) solution is directly incubated on the APTES-functionalized substrate. After a predetermined duration, the slide is rinsed thoroughly with DI water and observed by fluorescence microscopy. The exposure time is 307 ms.

Fluorescent Immunoassay. The experiment can be divided in three steps: the glass substrate functionalization with APTES, priming with 2019-nCoV antigen and the analyte

https://doi.org/10.1021/acs.analchem.2c03877
Anal. Chem. 2023, 95, 6253−6260

detection itself. When acoustic streaming is used, only the analyte detection is accelerated.

Substrate Priming. The assay begins with a priming step where 0.1 mg/mL 2019-nCoV (SARS-CoV-2) Spike (S) Protein (His-Avi) are incubated for 30 min at 25 °C on the APTES-functionalized glass substrate. Accordingly, the amount of spike protein used for each 2 μL droplet is 0.2 μg. In order to prevent nonspecific adsorption of other proteins on remaining APTES sites, the substrate is then immersed in a solution of 5% skim milk diluted with 0.5% Tween Phosphate Buffer Saline (PBST) for 30 min at 25 °C.

Analyte Detection. Before the assay, the optimal antibody concentration for comparison between diffusion and acoustic mixing is determined by a pure diffusion titer assay described in Supplementary Note 1 in the Supporting Information (SI). We find that the fluorescent immunoassay can detect antibody concentrations ranging from 0.06 to 1.77 ng/mL of SARS-CoV-2 (2019-nCoV) Spike Neutralizing Antibody. A concentration of 0.76 ng/mL was selected for our experiments. Primary antibody specificity, secondary antibody specificity and blank comparison results are shown in SI Supplementary Note 2.

In our experiments, the target analyte is suspended in a 2 μL droplet. Acoustic streaming mixing is active during the whole immunoassay. A solution of SARS-CoV-2 (2019-nCoV) Spike Neutralizing Antibody is first incubated on the substrate, then thoroughly rinsed with deionized (DI) water. The secondary antibody (0.2 mg/mL FITC * Goat Anti-Mouse lgG (H+L)) is then incubated on the substrate and rinsed thoroughly with DI water. Overall, 0.4 μg of secondary antibody is used for each droplet. To evaluate the amount of adsorbed antibody, fluorescence microscopy images of the sensor are recorded, and the average fluorescence intensity is computed with ImageJ.

Generation of Acoustic Streaming. Rayleigh acoustic streaming is powered by the shearing motion of acoustic waves at the interface between a solid and a fluid. In our Rayleigh acoustic streaming experiments, the acoustic power is provided by a piezoelectric transducer glued to the glass slide. Eckart acoustic streaming is powered by the dissipation of acoustic waves in the bulk of the fluid. In our Eckart acoustic streaming experiments, the acoustic power is provided by slanted interdigital transducer (IDT). In both of cases the droplet is located several centimeters away from the acoustic transducer. The acoustic vibrations are then transmitted through the solid to the liquid, where they accumulate due to acoustic resonance.

Electroacoustic Setup for Rayleigh Streaming. As shown in Figure 1(b), a lead zirconate titanate (PZT) piezoelectric disc is glued to the edge of a 50 × 50 × 1.8 mm^3 glass slide using a cyanoacrylate glue. To enhance repeatability, we have used a 3D-printed template to fix the position of glass substrate and PZT disc and press it using a binder clip, as shown in SI Supplementary Note 3. The disc is powered by an AG1021 (T&C) radiofrequency power amplifier connected to a signal generator (2207B, Picoscope). The excitation frequency was set to 800 kHz and the power output from the amplifier regulated to 2 W. During vibrometry experiments, the AG1021 was replaced with a LZY-22+ amplifier (Minicircuits) because the AG1021 could not be transported to the vibrometer. The signal generator voltage amplitude was set to 2 V, and the transmitted power was measured to be 4.63, 4.80, and 4.95 W at 800, 830, and 860 kHz, respectively. The excited transducer generates Lamb waves that travel guided along the glass substrate and transmit their vibrations to the droplet.

Electroacoustic Setup for Eckart Streaming. In Eckart streaming experiments, the streaming is powered by a surface acoustic wave (SAW) radiating into the droplet. The SAW is generated using a slanted-fingers interdigitated transducer (IDT). The transducer is produced by evaporating 10 nm of chromium and 100 nm of gold on a 1 mm thick Y-128° cut of $LiNbO_3$. The IDT is then patterned by wet etching following standard UV photolithography recipes. In order to facilitate subsequent surface treatments, the substrate is coated with 100 nm of SiO_2 to make it chemically similar to glass.

The slanted finger IDT can generate SAW with frequencies ranging between 20 and 32 MHz, which enables the fine positioning of the SAW beam relative to the droplet center.[30] The IDT is powered by ZHL-5W-1 (Mini-circuits) power amplifier connected to a signal generator (AFG31000, Tektronix). The signal generator voltage amplitude was set to 200 mV, and the transmitted power was measured to be 2.13 W. The experimental setup is shown in SI Supplementary Note 4.

Laser Doppler Vibrometry. The vibration amplitude of the droplet is measured by a Laser Doppler Vibrometer (LDV). The vibrometer (shown in SI Supplementary Figure 6) is a home-built heterodyne Mach−Zehnder interferometer.[31] While it has scanning functions, it was used only to measure the vibration of the top of the droplet. The laser hits the apex of the droplet and bounces back through a 40× microscope lens. Thanks to its large numerical aperture, such high-magnification lens can collect light from many directions which makes it relatively insensitive to small misalignment errors between the droplet vibrating surface and the vibrometer. During the measurements, the focus is regularly adjusted by hand to compensate for the droplet evaporation. We save the response of voltage of the photodiode at different times and then compute its Fourier transform, as shown in SI Supplementary Figure 7. Finally, we can calculate the vibration amplitude by the method described in SI Supplementary Note 5. The droplet vibration amplitude (94 nm) being comparable to the laser wavelength (633 nm), the perturbation approach described in Royer et al.[31] was not suitable. The non-perturbative method is described in SI Supplementary Note 5. The PZT was controlled by amplifier Minicircuits LZY-22+ and Picoscope 2207B (2 V). During vibrometry characterization, the droplet profile was photographed by an auxiliary side-looking microscope.

Acoustic Mixing Assay. During acoustic mixing assays, a 2 μL droplet is placed on the substrate (Figure 1). The droplet composition varies depending on the assay and is given in the corresponding method section (immunoassay/laser vibrometry/particle tracking). To enhance repeatability, the droplet contact line is immobilized using a gold ring patterned by photolithography and made hydrophobic using 1-dodecanethiol. In immunoassays, the gold ring was replaced with a silicone ring made of polydimethysiloxane. Once the droplet is in position, the acoustic power is activated and the droplet content is mixed using acoustic waves for the entire duration of the incubation step. Once the assay is completed, the surface is rinsed with DI water and observed using fluorescence microscopy.

General Defocusing Particle Tracking (GDPT). In order to visualize the acoustic streaming, the droplet is seeded with 2 μm diameter fluorescent particles. An f = 200.0 mm cylindrical

https://doi.org/10.1021/acs.analchem.2c03877
Anal. Chem. 2023, 95, 6253−6260

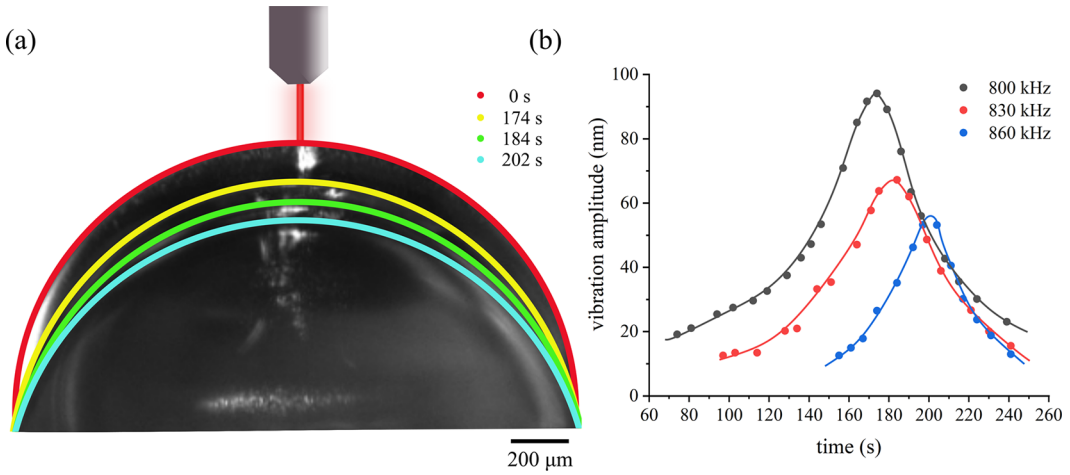

Figure 3. Measurements of the droplet surface vibrations by Laser Doppler Vibrometry (LDV). (a) Experimental profiles of the droplet at t = 174, 184, and 202 s. (b) Vibration amplitude over time with excitation frequencies of 800, 830, and 860 kHz.

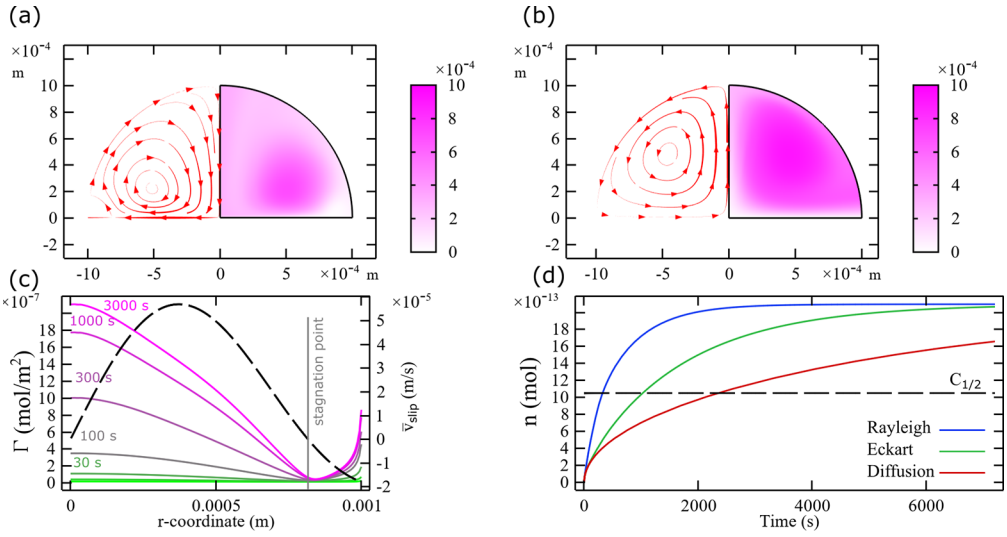

Figure 4. Numerical simulation of acoustic mixing in droplets. (a,b) Hydrodynamic flow streamlines (left) and analyte concentration profile (right) at t = 5 min in Rayleigh (a) and Eckart (b) mixing. The thickness of the streamlines is proportional to the flow velocity. (c) Radial distribution of adsorbed analyte (Γ) on the biosensor surface at different time points. To locate stagnation points, the slip velocity (eq 1) is given by the right axis. (d) Total amount of adsorbed analyte (n) on the sensor surface over time for various mass transfer methods. The dashed line indicates half the amount of analyte initially available. The droplet vibration amplitude is 62 nm.

lens (LJ1653RM-A, Thorlabs) is placed above the microscope objective to introduce a strong astigmatism that allows to calculate the out-of-plane location (z) of the particles based on the shape of their deformed image[32−35] (see SI Supplementary Note 6 for a more detailed explanation). These calculations of the particle position and subsequent reconstruction of the particle trajectories across multiple video frames are done using a Matlab implementation of the general defocus particle tracking (GDPT) method.[33]

Simulation of Acoustic Streaming and Mass Transfer. Compared to surface acoustic wave (SAW) driven Eckart streaming,[36−38] Rayleigh streaming in sessile droplets has received a limited attention. Peng et al.[39] have used a perturbation method to compute the acoustic streaming in two dimensions. In their paper, they resolve the viscoacoustic boundary layer to calculate the acoustic forcing. This requires a very fine mesh to capture all the details of this boundary layer[40] and therefore this method is restricted to two-dimensional models due to computer memory limitations. Here, we use the equivalent slip velocity as given by eq 1 to simulate acoustic streaming in three dimensions. For a given radial standing acoustic velocity field $\tilde{v}_r(t, r) = \tilde{V}_r(r)\sin(\omega t)$, Nyborg provides an expression of the slip velocity $\overline{v}_{slip}$ in the axisymmetric incompressible case.[16] In SI Supplementary Note 7, we show that this expression is also valid in the compressible case:

$$\overline{v}_{slip} = -\frac{3}{8\omega}(\partial_r \tilde{V}_r^2)\big|_{wall} - \frac{1}{2r\omega}(\tilde{V}_r^2)\big|_{wall} \quad (1)$$

It should be noted that the expression by Nyborg is appropriate when there is only tangential motion at the solid surface. Our model is a simple estimate of the actual process and assumes an infinite impedance mismatch between solid, liquid, and air. Therefore, only acoustic modes in water are considered. Compared to water, the acoustic impedance of glass or lithium niobate is very large, and therefore those solids can be considered to be infinitely hard boundaries (0 normal velocity) in first approximation. This allows us to use Nyborg

https://doi.org/10.1021/acs.analchem.2c03877
Anal. Chem. 2023, 95, 6253−6260

expressions here. Nevertheless, the experimental Q-factor is only 13, which suggests that transmitted waves between the solid and the fluid could be as large as 7% of the reflected ones. More refined models can be used to simulate the effect of normal vibrations, such as in refs 41 and 12.

The simulations are implemented with Comsol multiphysics using two-dimensional axisymmetric finite element models, using laminar flow (creeping flow) and mass transfer of dilute species modules. First, the acoustic field in the droplet is estimated based on the LDV calibration (see SI Supplementary Note 5), and the associated velocity field $\tilde{V}_r(r)$ is input in the model (SI Supplementary Note 8). The acoustic streaming is then computed from eq 1 using a stationary solver for the laminar flow equations. Next, this streaming field is used as input for a time-dependent convective mass-transfer and reaction problem. In the latter, antibody adsorption is simulated as a fast irreversible reaction. In first approximation, a typical antibody diffusivity is taken as 4×10^{-11} m^2/s.[42]

RESULTS AND DISCUSSION

Rayleigh Acoustic Streaming in Droplets. We first optimize acoustic excitation to maximize the acoustic streaming velocity. For water droplets on glass, the velocity of the acoustic streaming is proportional to the ultrasonic energy density in the liquid. In high-frequency Eckart streaming experiments, the acoustic energy is stored in whispering gallery modes that drive a fast acoustic streaming.[38] Provided that the acoustic wavelength is much shorter than the droplet size, these modes are insensitive to the ultrasonic frequency and the exact geometry of the droplet. However, at low frequencies characteristic of Rayleigh streaming, the acoustic wavelength becomes comparable to the droplet and energy can only be stored in discrete resonant frequency modes. At these frequencies, the acoustic field intensity peaks, which leads to the strongest acoustic streaming. However, due to evaporation, the droplet volume and contact angle change over time, and so does the resonance frequency. The experimental droplet profiles at three different stages of evaporation are shown as dotted lines in Figure 3(a), in which the red profile is the initial state of the droplet. Figure 3(b) shows the experimental vibration amplitude of the droplet apex over time for a given excitation frequency. All the curves feature a peak that indicates the onset of acoustic resonance. For instance, a droplet excited at 800 kHz becomes resonant after 174 s of evaporation, whereas a droplet excited at 860 kHz resonates after 202 s. Conversely, it is conceivable that a droplet could be maintained resonant at all times by dynamically adjusting the frequency. Furthermore, for a given droplet geometry (say t = 160 s), the excitation amplitude is divided by 2 when the frequency increases by 30 kHz, which gives an estimated $Q = f/\Delta f \approx 13$ where Δf is the half-maximum full bandwidth (60 kHz) and f is the resonance frequency (800 kHz). This suggests that the droplet behaves essentially as an acoustic resonator such that the acoustic field in the droplet can be reduced to the resonant mode.

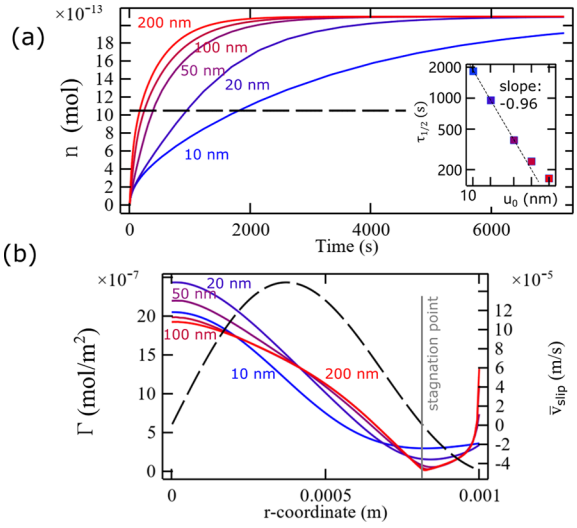

Figure 5. (a) Total amount of adsorbed analyte (n) on the sensor surface over time for various droplet surface vibration amplitude (u_0). The dashed line indicates half the amount of analyte initially available. Inset: scaling of the adsorption characteristic time $\tau_{1/2}$ depending on the droplet vibration amplitude. (b) Effect of the droplet surface vibration amplitude (u_0) on the radial distribution of adsorbed analyte (Γ) on the biosensor surface after 2 h. To locate stagnation points, the slip velocity (eq 1) for a droplet vibration amplitude of 100 nm is given by the dashed line (right axis).

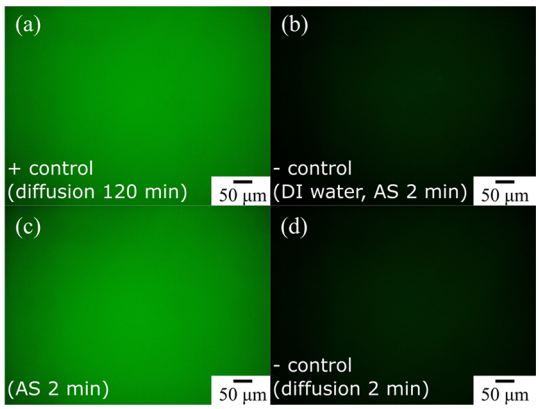

Figure 6. Fluorescence microscopy images after incubation in different conditions (a) 0.2 mg/mL FITC * Goat Anti-Mouse lgG (H+L) after 2 h of diffusion at 37 °C, (b) deionized (DI) water after 2 min of Rayleigh acoustic streaming (AS), (c) 0.2 mg/mL FITC * Goat Anti-Mouse lgG (H+L) after 2 min of Rayleigh acoustic streaming (d) 0.2 mg/mL FITC * Goat Anti-Mouse lgG (H+L) after 5 min of diffusion.

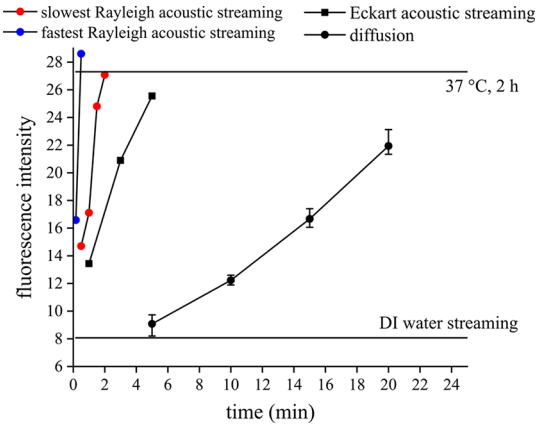

Figure 7. Comparison of adsorption kinetics of 0.2 mg/mL FITC * Goat Anti-Mouse lgG (H+L) with and without acoustic mixing. The limit of detection is obtained from DI water.

https://doi.org/10.1021/acs.analchem.2c03877
Anal. Chem. 2023, 95, 6253−6260

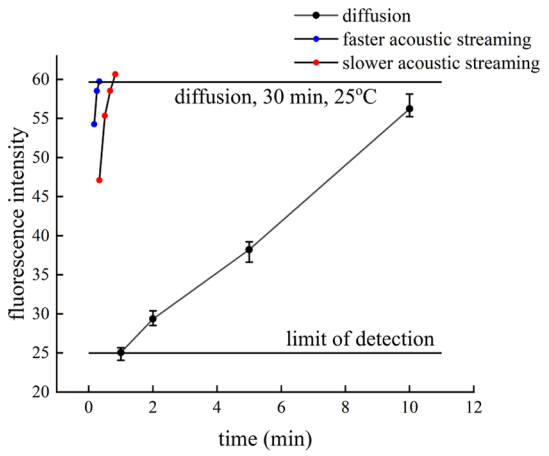

Figure 8. Acceleration of an immunofluorescent SARS-CoV-2 (2019-nCoV) Spike Neutralizing Antibody detection assay by Rayleigh acoustic streaming. The incubation time for each antibody is kept the same, and is indicated on the horizontal axis. Therefore, a 10 min value on the axis indicates a total detection duration of 20 min. Limit of detection is obtained from the inflection point of the titer curve (SI Supplementary Note 1).

In order to visualize the acoustic streaming, the three-dimensional trajectory of 2 μm diameter fluorescent particles dispersed in the droplet is reconstructed by GDPT and the computed velocity field is shown in Figure 2(b). The poloidal flow compares qualitatively well to our numerical simulation. The experimental average velocity is 10 μm/s, which is of similar magnitude to the 9.8 μm/s obtained from simulations of a droplet vibration amplitude of 62 nm based on vibrometer data (see SI Supplementary Note 5).

Acceleration of Mass Transfer by Rayleigh Acoustic Streaming. Having validated the numerical method, we use our model to compare the mass transfer performance of pure diffusion, Eckart streaming and Rayleigh streaming. For the sake of comparison, the average velocity of Eckart streaming is set to the same value as Rayleigh streaming (9.8 μm/s). The resulting velocity fields and concentration profiles after 5 min are shown in Figure 4(a,b) (the concentration in the pure diffusion case is shown in SI Supplementary Figure 10). Concentration distribution in droplets in each case after 5 min indicates that the analyte is mainly depleted near the solid in the case of Eckart streaming and diffusion, whereas Rayleigh streaming has a much better uniformity. Simulations also reveal that the spatial distribution of adsorbed analyte (adsorption profile) evolves over time (Figure 4(c)). The adsorption is mainly concentrated at the stagnation point at the center of the droplet, where streaming intensity is minimum. This is similar to the case of Rayleigh-streaming-enhanced heat transfer between two plates held at constant temperature where heat transfer primarily occurs at the hydrodynamic velocity nodes.[43] However, the adsorption minimum is located at another stagnation point. We believe that there is almost no analyte adsorbed there because the inward poloidal flow ensures that all analyte is adsorbed before reaching this second stagnation point. In order to compare the mixing performance of Eckart acoustic streaming, Rayleigh acoustic streaming and pure diffusion Figure 4(d), we define $\tau_{1/2}$ as the time it takes to transport half the analyte to the solid surface. Diffusion takes $\tau_{1/2}$ = 2357 s (39 min), SAW induced Eckart streaming shortens this process to $\tau_{1/2}$ = 1026 s (≈17 min) and Rayleigh streaming takes $\tau_{1/2}$ = 322 s (≈5 min). Therefore, Rayleigh streaming mass transfer is three times faster than Eckart mixing at equal average flow velocity in the droplet. Therefore, a mass-transfer limited assay would be three times shorter using Rayleigh streaming than when using Eckart streaming.

Finally, we use the simulations to evaluate the effect of the excitation amplitude on $\tau_{1/2}$ (Figure 5(a)). For small oscillation amplitude (≲50 nm), we obtain a linear relationship, similar to Vainshtein et al.[43] At high amplitude, the adsorption kinetic differs from the high Peclet asymptotic regime of Vainshtein et al.[43] In their work, adsorption is mainly concentrated at the hydrodynamic nodes, whereas in the case of the droplet the streaming stagnation points are more ambiguous and can either be the location of maxima or minima of adsorption (Figure 5(b)).

Next, we evaluate experimentally the acceleration of protein mass transfer to the surface. A fluorescent antibody (FITC * Goat Anti-Mouse lgG (H+L)) able to bind to silanized glass is used to assess mass transfer enhancement due to acoustic streaming. The intensity of fluorescence after different conditions of incubation is shown in Figure 6. A positive and negative control samples are prepared to bracket the pixel intensity value between the noise floor and the maximum expected intensity. The positive control (Figure 6(a)) is the fluorescence obtained after immersing the slide in the antibody solution for 2 h at 37 °C. The negative control (Figure 6(b)) is the fluorescence image of a pure deionized (DI) water sample after 2 min of Rayleigh acoustic streaming. Finally, the fluorescence level after 2 min of antibody adsorption with and without Rayleigh streaming are shown in Figure 6(c,d), respectively. The droplet without Rayleigh acoustic mixing looks similar to the negative control (DI water), whereas the droplet that was acoustically mixed looks like the positive control, indicating a saturated adsorption.

The variation of fluorescence intensity over time is shown in Figure 7 for pure diffusion, Eckart and Rayleigh acoustic streaming cases. In the case of pure diffusion, the fluorescence intensity increases steadily, but after 20 min the droplet is completely evaporated and yet the fluorescence intensity remains weaker than the positive control (2 h, 37 °C). In contrast, Rayleigh acoustic streaming mixed droplets reach the saturation value within 30 s (fastest sample) to 2 min (slowest sample), the dispersion being due to the sensitive interplay

Table 1. Comparison of Adsorption Speed up between Eckart and Rayleigh Mixing

method	droplet volume (μL)	fluorescent species	acoustic duration	speedup	ref
Eckart	"microliter"	2 μm beads	5 min 40 s	NA	19
Eckart	20	fluorescent carcinoembryonic antibody	10 min	12	45
Rayleigh	2	SARS-CoV-2 Spike Neutralizing Antibody	40 s	30	this work (Exp)
Eckart	2	NA	17 min	2.3	this work (Sim)
Rayleigh	2	NA	5 min	7.3	this work (Sim)

https://doi.org/10.1021/acs.analchem.2c03877
Anal. Chem. 2023, 95, 6253−6260

between droplet volume and resonance frequency (Figure 3). Even then, Rayleigh mixing remains at least 2.5 times faster (and up 10 times faster) than mixing based on Eckart streaming (5 min).

Acceleration of SARS-CoV-2 Detection with Acoustic Streaming. Droplet-based assays are known to reduce reagent use. For surface bioassays, the important metric is the surface concentration of each species, and therefore the total amount of reagent needed is proportional to the surface area of the droplet bottom or, in microplates, of the well bottom. The droplet used in this paper are 2 mm diameter, which is twice smaller than the well of a 96-well plate (5 mm) recommended for such assays. While antigen and secondary antibody concentration were not optimized, we note that 1.5 ng of SARS-CoV-2 Spike Neutralizing Antibody are required for this assay whereas 96-well plate protocols typically recommend 30 to 60 ng per well.[44]

We demonstrate the acceleration of a bioassay to measure the level of SARS-CoV-2 specific antibody (SARS-CoV-2 Spike Neutralizing Antibody) in a liquid sample (here 0.5% Tween Phosphate Buffer Saline (PBST)). The SARS-CoV-2 specific antibody (primary antibody) specifically binds to an antigen on the surface (2019-nCoV Spike(S) Protein (His-Avi)). This primary antibody is then detected by a fluorescent secondary antibody (FITC * Goat Anti-Mouse lgG (H+L))). Therefore, this experiment involves two incubation steps. For the sake of simplicity, both steps have the same duration.

The fluorescence levels depending on the incubation method (diffusion or Rayleigh acoustic mixing) are shown in Figure 8. Accordingly, 20 s of acoustic mixing yields fluorescence levels comparable to 10 min of diffusion. This shows that Rayleigh streaming is a highly efficient method to accelerate surface bioassays. It is also instructive to compare Rayleigh streaming results to previous immunoassays using Eckart streaming[19,45] that needed 5 to 10 min of mixing (or "sample concentration") to complete. Even though these assays did not use the exact same experimental conditions (see Table 1), the speed up offered by Rayleigh streaming is approximately three times larger than Eckart mixing, both in simulations and experiments.

CONCLUSIONS

Accelerating fluid mixing in droplet is a key problem to address to improve biosensor speed without compromising the reagent consumption. In this paper, we propose to use Rayleigh acoustic streaming to bypass the hydrodynamic boundary layer that has long limited SAW-based droplet mixing. Our simulations and experiments unveil the three-dimensional hydrodynamic flow in the droplet. The simulations also reveal the adsorption profile of the analyte in the droplet and the scaling of the adoption with the acoustic excitation amplitude. Experimentally, we demonstrate that Rayleigh streaming can shorten the detection time of FITC * Goat Anti-Mouse lgG (H+L) by three-fold compared to Eckart streaming and also shorten the SARS-CoV-2 Spike Neutralizing Antibody detection time by up to 30 times compared to diffusion, which reduces the detection time below 40 s. The application of acoustic streaming in immunoassays provides the possibility for rapid detection of emergent pathogens.

ASSOCIATED CONTENT

Supporting Information

The Supporting Information is available free of charge at https://pubs.acs.org/doi/10.1021/acs.analchem.2c03877.

Primary antibody titer assay; immunofluorescence assay specificity; 3D-printed template; experimental setup photographs; laser doppler vibrometry (LDV) non-perturbative analysis; general defocusing particle tracking (GDPT) calibration; generalization of Nyborg formula for axisymmetric acoustic streaming; acoustic field in the droplet; and simulated concentration profiles (PDF)

AUTHOR INFORMATION

Corresponding Authors

Gary Wong − *Viral Hemorrhagic Fevers Research Unit, CAS Key Laboratory of Molecular Virology and Immunology, Institut Pasteur of Shanghai, Chinese Academy of Sciences, Shanghai 200031, P. R. China*; Email: garyckwong@ips.ac.cn

Jia Zhou − *ASIC and System State Key Laboratory, School of Microelectronics, Fudan University, Shanghai 200433, P. R. China*; Email: jia.zhou@fudan.edu.cn

Antoine Riaud − *ASIC and System State Key Laboratory, School of Microelectronics, Fudan University, Shanghai 200433, P. R. China*; orcid.org/0000-0001-8323-706X; Email: antoine.riaud@gmail.com

Authors

Qi Wang − *ASIC and System State Key Laboratory, School of Microelectronics, Fudan University, Shanghai 200433, P. R. China*; orcid.org/0000-0002-2833-9175

Zhe Ding − *Viral Hemorrhagic Fevers Research Unit, CAS Key Laboratory of Molecular Virology and Immunology, Institut Pasteur of Shanghai, Chinese Academy of Sciences, Shanghai 200031, P. R. China; University of Chinese Academy of Sciences, Beijing 100049, P. R. China*

Complete contact information is available at: https://pubs.acs.org/10.1021/acs.analchem.2c03877

Notes

The authors declare no competing financial interest.

ACKNOWLEDGMENTS

This work was supported by the National Natural Science Foundation of China with Grant Nos. 62274039 and 12004078; State Key Lab of ASIC and System, Fudan University Nos. 2021MS001, 2021MS002, and 2020KF006; Science and Technology Commission of Shanghai Municipality No. 22QA1400900 and No. 22WZ2502200. This project was supported by the Ministry of Science and Technology of China (Grant No. 2021YFC0863400, 2022YFE0114700), G4 funding from Institut Pasteur, Fondation Merieux and Chinese Academy of Sciences to G.W., and the International Affairs Department of the Institut Pasteur of Paris.

REFERENCES

(1) Gervais, T.; Jensen, K. F. *Chemical engineering science* **2006**, *61*, 1102.

(2) Hansen, R.; Bruus, H.; Callisen, T. H.; Hassager, O. *Langmuir* **2012**, *28*, 7557.

(3) Pereiro, I.; Fomitcheva-Khartchenko, A.; Kaigala, G. V. *Anal. Chem.* **2020**, *92*, 10187.
(4) Mugele, F.; Baret, J.-C.; Steinhauser, D. *Appl. Phys. Lett.* **2006**, *88*, 204106.
(5) Samiei, E.; de Leon Derby, M. D.; Van den Berg, A.; Hoorfar, M. *Lab Chip* **2017**, *17*, 227.
(6) Park, J.; Ryu, J.; Sung, H. J.; Kim, H. *J. Colloid Interface Sci.* **2020**, *561*, 408.
(7) Wixforth, A. *Superlattices Microstruct.* **2003**, *33*, 389.
(8) Zhang, N.; Zuniga-Hertz, J. P.; Zhang, E. Y.; Gopesh, T.; Fannon, M. J.; Wang, J.; Wen, Y.; Patel, H. H.; Friend, J. *Lab Chip* **2021**, *21*, 904.
(9) Zauhar, G.; Starritt, H.; Duck, F. *British journal of radiology* **1998**, *71*, 297.
(10) Garg, N.; Boyle, D.; Randall, A.; Teng, A.; Pablo, J.; Liang, X.; Camerini, D.; Lee, A. P. *Lab Chip* **2019**, *19*, 1524.
(11) Ghanem, M. A.; Maxwell, A. D.; Wang, Y.-N.; Cunitz, B. W.; Khokhlova, V. A.; Sapozhnikov, O. A.; Bailey, M. R. *Proc. Natl. Acad. Sci. U. S. A.* **2020**, *117*, 16848.
(12) Vanneste, J.; Bühler, O. *Proceedings of the Royal Society A: Mathematical, Physical and Engineering Sciences* **2011**, *467*, 1779.
(13) Sadhal, S. *Lab Chip* **2012**, *12*, 2600.
(14) Eckart, C. *Physical review* **1948**, *73*, 68.
(15) Rayleigh, L. *Phil. Trans. R. Soc.* **1884**, *175*, 1.
(16) Nyborg, W. L. *J. Acoust. Soc. Am.* **1958**, *30*, 329.
(17) Bach, J. S.; Bruus, H. *J. Acoust. Soc. Am.* **2018**, *144*, 766.
(18) Shilton, R.; Tan, M. K.; Yeo, L. Y.; Friend, J. R. *J. Appl. Phys.* **2008**, *104*, 014910.
(19) Bourquin, Y.; Reboud, J.; Wilson, R.; Zhang, Y.; Cooper, J. M. *Lab Chip* **2011**, *11*, 2725.
(20) Renaudin, A.; Chabot, V.; Grondin, E.; Aimez, V.; Charette, P. G. *Lab Chip* **2010**, *10*, 111.
(21) Salman, H.; Haynes, P. *Phys. Fluids* **2007**, *19*, 067101.
(22) Lebedev, V.; Turitsyn, K. *Phys. Rev. E* **2004**, *69*, 036301.
(23) Li, X.; Huffman, J.; Ranganathan, N.; He, Z.; Li, P. *Anal. Chim. Acta* **2019**, *1079*, 129.
(24) Zhang, C.; Brunet, P.; Royon, L.; Guo, X. *Chemical Engineering Journal* **2021**, *410*, 128252.
(25) Rasouli, M. R.; Tabrizian, M. *Lab Chip* **2019**, *19*, 3316.
(26) Chen, H.; Chen, C.; Bai, S.; Gao, Y.; Metcalfe, G.; Cheng, W.; Zhu, Y. *Nanoscale* **2018**, *10*, 20196.
(27) Meng, L.; Liu, X.; Wang, Y.; Zhang, W.; Zhou, W.; Cai, F.; Li, F.; Wu, J.; Xu, L.; Niu, L.; et al. *Advanced Science* **2019**, *6*, 1900557.
(28) Marin, A.; Rossi, M.; Rallabandi, B.; Wang, C.; Hilgenfeldt, S.; Kähler, C. J. *Physical Review Applied* **2015**, *3*, 041001.
(29) Bengtsson, M.; Laurell, T. *Anal. Bioanal. Chem.* **2004**, *378*, 1716.
(30) Gu, Y.; Chen, C.; Mao, Z.; Bachman, H.; Becker, R.; Rufo, J.; Wang, Z.; Zhang, P.; Mai, J.; Yang, S.; Zhang, J.; Zhao, S.; Ouyang, Y.; Wong, D. T. W.; Sadovsky, Y.; Huang, T. J.; et al. *Science advances* **2021**, *7*, No. eabc0467.
(31) Royer, D.; Dieulesaint, E. *Applied physics letters* **1986**, *49*, 1056.
(32) Muller, P. B.; Rossi, M.; Marin, A.; Barnkob, R.; Augustsson, P.; Laurell, T.; Kaehler, C. J.; Bruus, H. *Phys. Rev. E* **2013**, *88*, 023006.
(33) Barnkob, R.; Kähler, C. J.; Rossi, M. *Lab Chip* **2015**, *15*, 3556.
(34) Barnkob, R.; Rossi, M. *J. Open Res. Software* **2021**, *9* (1), 22 DOI: 10.5334/jors.351.
(35) Rossi, M.; Marin, A.; Kähler, C. J. *Phys. Rev. E* **2019**, *100*, 033103.
(36) Shiokawa, S.; Matsui, Y.; Ueda, T. *Japanese journal of applied physics* **1990**, *29*, 137.
(37) Raghavan, R. V.; Friend, J. R.; Yeo, L. Y. *Microfluid. Nanofluid.* **2010**, *8*, 73.
(38) Riaud, A.; Baudoin, M.; Bou Matar, O.; Thomas, J.-L.; Brunet, P. *J. Fluid Mech.* **2017**, *821*, 384.
(39) Peng, T.; Li, L.; Zhou, M.; Jiang, F. *Sensors* **2022**, *22*, 1269.
(40) Muller, P. B.; Barnkob, R.; Jensen, M. J. H.; Bruus, H. *Lab Chip* **2012**, *12*, 4617.
(41) Manor, O.; Yeo, L. Y.; Friend, J. R. *Journal of fluid mechanics* **2012**, *707*, 482.
(42) Pokrić, B.; Pučar, Z. *Analytical biochemistry* **1979**, *93*, 103.
(43) Vainshtein, P.; Fichman, M.; Gutfinger, C. *Int. J. Heat Mass Transfer* **1995**, *38*, 1893.
(44) *Microplates for enzyme linked immunosorbent assays (elisa)*, https://www.dutscher.com/data/pdf_guides/en/Guide_de_selection_ELISA_Microlon_Greiner_Bio-One.pdf, accessed: 2022−08−31.
(45) Liu, J.; Li, S.; Bhethanabotla, V. R. *ACS sensors* **2018**, *3*, 222.

Recommended by ACS

Evaluation of Analyte Transfer between Microfluidic Droplets by Mass Spectrometry
Emory M. Payne, Robert T. Kennedy, *et al.*
MARCH 02, 2023
ANALYTICAL CHEMISTRY
READ

Auto Flow-Focusing Droplet Reinjection Chip-Based Integrated Portable Droplet System (iPODs)
Fengyi Liu, Bo Ma, *et al.*
APRIL 13, 2023
ANALYTICAL CHEMISTRY
READ

Connected Droplet Shape Analysis for Nanoflow Quantification in Thin Electroosmotic Micropumps and a Tunable Convex Lens Application
Sai Siva Kare, John Desmond Finan, *et al.*
FEBRUARY 10, 2023
LANGMUIR
READ

Bent-Capillary-Centrifugal-Driven Monodisperse Droplet Generator with Its Application for Digital LAMP Assay
Ziwei Zhang, Meijia Zhu, *et al.*
JANUARY 23, 2023
ANALYTICAL CHEMISTRY
READ

Get More Suggestions >

https://doi.org/10.1021/acs.analchem.2c03877
Anal. Chem. 2023, 95, 6253−6260